Available at www.sciencedirect.com

ScienceDirect

journal homepage: www.elsevier.com/locate/issn/15375110

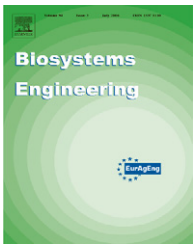

Research Paper: PH—Postharvest Technology

Experimental methods for evaluating heating uniformity in radio frequency systems

S. Wang, K. Luechapattanaporn, J. Tang*

Department of Biological Systems Engineering, Washington State University, 213 L. J. Smith Hall, Pullman, WA 99164-6120, USA

ARTICLE INFO

Article history:
Received 19 October 2007
Accepted 31 January 2008
Available online 17 March 2008

Heating uniformity is one of the most important considerations in developing radio frequency (RF) systems and processes in heating applications. Two different loads were used in this study to evaluate heating uniformity in a 12 kW, 27.12 MHz pilot-scale RF system with plate applicators. One method involved the use of a custom-designed water load, while the other used polyurethane foam. For the water load, 24 thermocouples simultaneously measured final temperatures of water and 1% carboxymethylcellulose (CMC) solution in both horizontal and vertical planes. Regulating the air gaps between the top electrode and the water or CMC samples resulted in different power couplings in the heating load ranging from 5.5 to 10 kW and corresponding heating rates of 5.3–9.4 °C min^{-1}. The hottest spot was always located near the electrode centre. The temperature difference between the front and back sides of the RF cavity was less than 2 °C, but the difference between the right and left sides was as much as 10 °C. A relatively large zone was defined in the centre where the temperature difference was less than 4 °C. A symmetric design of the inductance positions and feeding strips improved the heating uniformity. The temperature distribution after symmetric design was further confirmed in polyurethane foams using a thermal imaging camera. Further research is needed to improve the heating uniformity with the help of computer modelling.

1. Introduction

Radio frequency (RF) energy has been used in industrial applications for curing or drying of wood, textiles, paper and cardboard, and for post-back drying in the biscuit industry (Mataxas and Clee, 1993; Jones, 1997). Small-scale RF systems have been extensively used in laboratory studies for disinfesting agricultural commodities (Headlee and Burdette, 1929; Frings, 1952; Nelson and Payne, 1982; Hallman and Sharp, 1994; Nelson, 1996). But practical applications for insect control have not been implemented due to comparatively inexpensive chemical fumigation (Nelson, 1972). Because of new regulatory actions against chemical fumigation, interest in using RF energy as an alternative physical treatment method has increased recently (Tang et al., 2000). For example in research, RF energy has been used to control insect pests in heat-sensitive agricultural commodities, including cherries (Ikediala et al., 2002) and walnuts (Wang et al., 2001, 2002, 2007a, 2007b; Mitcham et al., 2004). The treatment margin for achieving effective insect control with acceptable product quality is very limited for thermal treatments even in a small container, especially for fresh fruits (Birla et al., 2005). It is important to determine and improve the heating uniformity of RF-treated products to ensure the efficacy of the treatments and scaling-up to commercial applications.

RF energy interacts directly with the agricultural products and can rapidly increase their temperature volumetrically. A major concern in developing an RF treatment protocol is the heating uniformity in the treated samples (Wang et al., 2005).

*Corresponding author. Tel.: +1 509 3357950; fax: +1 509 3352722.
E-mail address: shaojin_wang@wsu.edu (S. Wang).
1537-5110/$ - see front matter © 2008 IAgrE. Published by Elsevier Ltd. All rights reserved.
doi:10.1016/j.biosystemseng.2008.01.011

Temperature variations after RF heating may result from the different properties of samples and a non-uniform electromagnetic field (Wang et al., 2003a; Birla et al., 2004). Resolving uneven electromagnetic fields is an important challenge during development of postharvest insect control for fresh fruits because a few degrees' deviation from the target temperature causes either insect survival or quality deterioration. It is desirable to develop appropriate means for direct measurement of heating uniformity for a given RF unit and make reasonable suggestions as to how the manufacturer might improve the cavity and electrode configuration.

Many studies have been conducted to determine power distributions in microwave heating using a voltage meter, thermal imaging (Ma et al., 1995; Zhou et al., 1995) and chemical markers (Wang et al., 2003b). These methods have different limitations in use, e.g. only the surface temperature is measured by thermal imaging, and sample temperatures are indirectly deduced from colour patterns created by chemical markers. Jia (1993) used a water container (38 cm × 40 cm) to validate microwave power distributions in a microwave applicator obtained by numerical simulation. Zhong et al. (2003) evaluated the temperature distribution of tap water and 1% carboxymethylcellulose (CMC) solutions in a continuous flow RF heating system. Up to now, no direct measurements of temperature distributions in a large-scale RF system have been reported to guide RF cavity design or to validate computer simulation results.

The objectives of this study were: (1) to measure the dielectric properties of tap water and 1% CMC solutions and use these solutions as loads to evaluate RF heating uniformity; (2) to determine experimentally the heating uniformity in horizontal and vertical planes using tap water and 1% CMC solutions; and (3) to evaluate the heating uniformity improvement using the water load after the symmetric design of feeding and inductance positions on the top electrode and confirm the temperature distribution using a polyurethane foam.

2. Materials and methods

2.1. RF systems

A 12 kW, 27.12 MHz pilot-scale RF system (Strayfield Fastran with E-200, Strayfield International Limited, Wokingham, UK) was used to heat the tap water and 1% CMC solutions in a heating load (Fig. 1). The load was heated between two parallel plate electrodes (104 cm × 80 cm). The gap between the electrode plates was adjusted to have suitable RF power coupled to the samples. There was no air circulation in the RF cavity. Before the tests the distance between the top and bottom electrode plates was adjusted to be constant (variation <1 mm) over the entire electrode plate surface to avoid the effect of gap variations between the electrode plates on the electromagnetic field. The original positions of the feed strips and conductors on the top electrode are shown in Fig. 2.

2.2. Measurement of dielectric and ionic properties

The dielectric properties of samples can provide general information on selecting a desired heating rate and determining the optimum thickness of the samples in RF heating. Before the dielectric property measurement, a 1% sodium CMC solution (TIC Pre-Hydrated TICALOSE® CMC 6000 Powder, Belcamp, Maryland) was prepared by mixing CMC powder with tap water (used without purification). The solution was left at room temperature for 2 days to ensure an even mixture before tests. The dielectric properties of tap water and 1% CMC solutions were measured by an open-ended coaxial probe technique with an impedance analyzer (Model 4291B, Innovative Measurement Solutions Inc., Santa Clara, CA). A detailed description of the system can be found in Wang et al. (2003a). The mean and standard deviation of the dielectric constant and loss factor were determined at 27.12 MHz at five temperatures (20, 30, 40, 50 and 60 °C) based on experimental data in two replicates. The penetration depth was calculated using the method reported in Wang et al. (2003a). The ionic conductivity of tap water and 1% CMC solutions was measured at 20 °C with an Economy Benchtop Conductivity meter (CON 500 Meter w/Probe, New Hyde Park, NY).

2.3. Heating container and temperature measurement system

The heating load consisting of 88 cups made of acrylic glass (Plexiglas) was developed for temperature distribution tests (Fig. 1). The loss factor of acrylic glass was about 2, which was

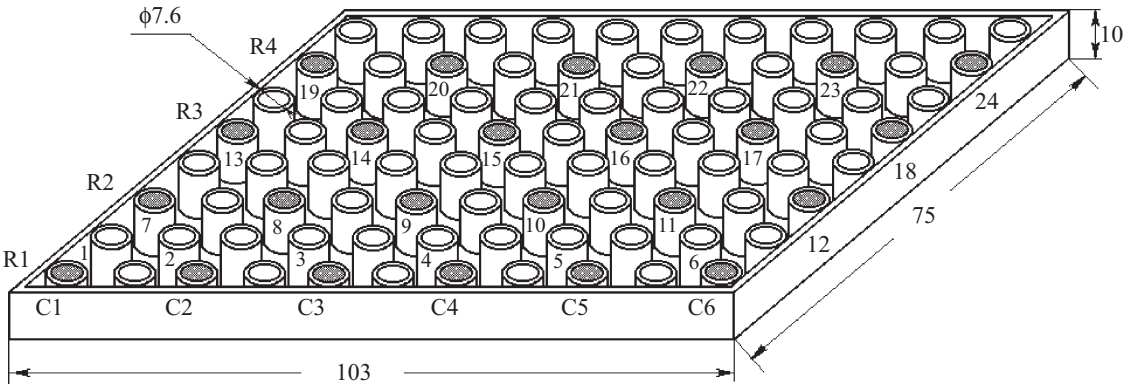

Fig. 1 – Heating load with 24 cups (in dark) in 4 rows and 6 columns for temperature distribution tests (all units are in cm).

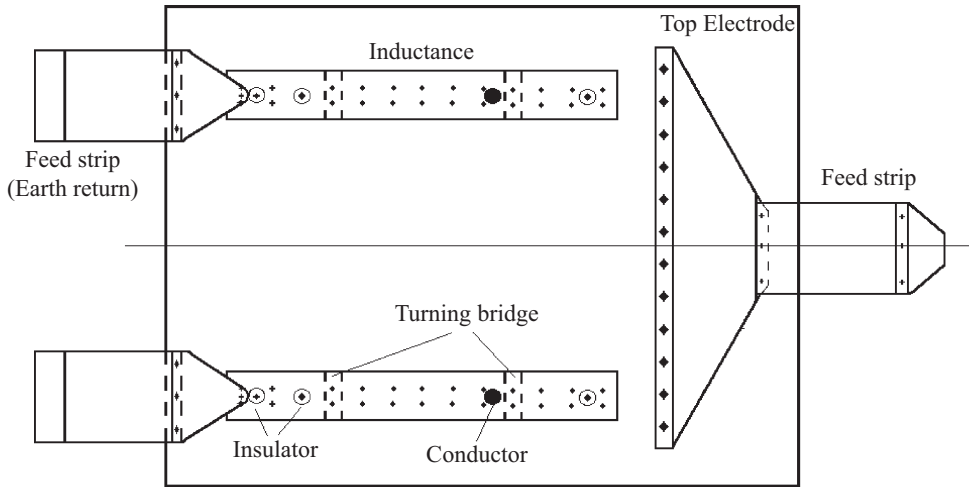

Fig. 2 – Schematic view of the original positions of feed strips and conductors on the top electrode.

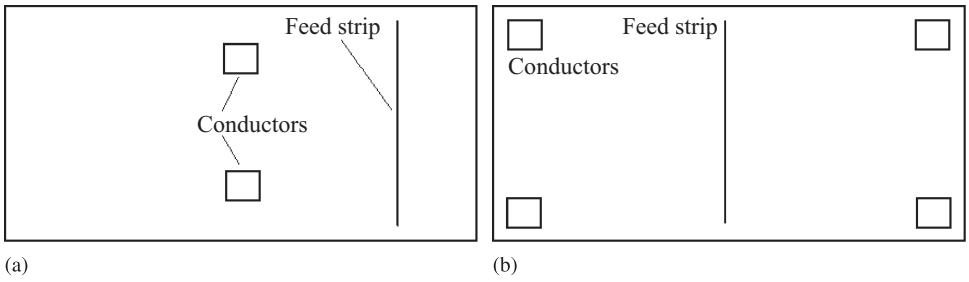

Fig. 3 – The positions of the feed strip and conductors that were attached to the top electrode of the RF unit: (a) original locations and (b) new symmetric locations.

significantly smaller than that of tap water (18–20 at 20 °C). Twenty-four cups were first filled with water and used to determine the horizontal temperature distribution. The load was placed directly on the bottom electrode in the centre of the electrode area. During heating, the water temperatures in the centre of cups 9, 10, 15 and 16 were monitored by fibre-optic temperature sensors (UMI, FISO Technologies Inc., Saint-Foy, Quebec, Canada). The RF system was turned off when the maximum water temperature reached 50 °C. After RF heating, the load was immediately pulled out of the cavity. A cover plate with 24 thermocouples was placed on the top of the load to measure simultaneously the water temperatures in the middle of the selected 24 cups using a data logger (DL2e, Delta-T Devices Ltd., Cambridge, UK). The 24 thermocouples (Type T, gage factor 36, Omega Engineering Inc., Stamford, CT) were calibrated in a water bath against a standard thermometer and were pre-mounted on a support pole on the cover plate at a height of 4.5 cm from the cup bottom. For vertical temperature profiles, 24 thermocouples were also used to measure three different depths in the eight selected cups. The temperatures at heights of 2.5, 4.5 and 6.5 cm in each cup in columns C3 and C4 were recorded at the same time (Fig. 1). The initial and final water temperatures in each of the 24 cups were sampled every second and recorded every 10 s.

2.4. *Experimental procedures*

For the original positions of conductors and feed strips (Fig. 3a), tap water was uniformly filled fully into the 24 cups at room temperature. The initial water temperature at room conditions in each cup was recorded by the data logger. The load was then placed in the centre of the electrode area. The RF power and the electrode gap were controlled to achieve a suitable heating rate. The RF heating was stopped when the water temperature displayed in the fibre-optic system was about 50 °C. The cover plate with 24 thermocouples connected to the data logger was placed on the container after pulling it from the cavity. After recording the temperature, the warm water in the cups was removed by vacuum and the container was cooled down for the next run.

In order to determine the effect of different loads on the horizontal temperature distribution, different numbers of samples (24, 16 and 4 cups) were used to analyse the heating uniformity using the same water load. The results were presented to compare the average and maximum differences in the cups.

Vertical temperature distributions were determined in 8 cups of the load located in columns C3 and C4 (Fig. 1). Temperatures at three levels in each cup were measured at the same time after stopping RF heating. The 24 temperatures

were used to provide the vertical temperature distribution. To eliminate the possible heat convection in the water load for vertical temperature testing, 1% CMC solutions were carefully filled into 24 cups at the same full level for determining the vertical temperature distribution. Because of temperature variations as a function of measurement time, the vertical temperature distribution in columns C3 and C4 2 min after insertion of the thermocouples was plotted using a contour graph for comparisons.

The asymmetric connections of the inductor and the power supply to the top electrode resulted in an uneven standing wave pattern across the applicator. To achieve a uniform RF field, a new symmetric design (Fig. 3b) was developed. The four conductors were installed at the four corners on the top electrode and the feed strip was moved to the centre. The four corner inductors allowed independent adjustment of the voltage at each corner. This step was intended to further improve the heating uniformity beneath the top plate electrode with the symmetric design of the four conductors. A Hewlett-Packard 8752C network analyzer (Agilent Technologies, Palo Alto, CA) was used to tune the natural frequency of the applicator. Simple loop antennas placed near the applicator and inductors permitted the measurement of reflection and transmission over a range of frequencies, from 1 to 100 MHz. The network analyser was useful in determining the size of the inductors needed during refitting. The tap water temperatures in 24 cups for the horizontal distribution in the symmetric design were compared with those in the original design.

To further verify the horizontal heating uniformity in the symmetric design, two sheets of polyurethane foams (81 cm × 61 cm × 5 cm), overlapping each other, were used as a load in the RF unit. The foam load method was used in Wang et al. (2007a) to indirectly evaluate the electromagnetic field intensity in industrial-scale RF systems. The initial temperatures were 22 °C after equilibrium under room conditions for at least 1 day. During the heating, the gap between the RF electrodes was adjusted to 160 mm, which resulted in 3.8 kW power. After RF heating for 3 min, the foams were immediately taken out of the RF cavity for temperature measurement. A horizontal surface temperature distribution in the central layer (by removing the upper polyurethane foam) was obtained using an infrared camera (Thermal CAM^{TM} SC-3000, N. Billerica, MA) having an accuracy ±2 °C. The thermal image with 45,056 individual temperature data was collected and used to plot a contour graph.

3. Results and analyses

3.1. Dielectric properties

The dielectric properties of tap water and 1% CMC solutions at 27.12 MHz are shown in Table 1. The dielectric constant of tap water and 1% CMC solutions decreased with increasing temperature but their dielectric loss factors increased with increasing temperature. The loss factor of 1% CMC solutions was almost four times that of tap water at each temperature, because the ionic conductivity dominated the dielectric loss factor at 27.12 MHz (Wang et al., 2003a; Zhong et al., 2003). The average values of the ionic conductivity of tap water and 1% CMC solutions were 330 and 1230 μS cm^{-1} at 20 °C, respectively. These values were comparable to those of 1% CMC solutions obtained by Zhong et al. (2003) and those for tap water in Pullman, WA in an early study (Ikediala et al., 2002). The penetration depths for tap water at temperatures from 20 to 60 °C were much larger than that of the cup radius (3.8 cm) and height (10 cm), suggesting that there would only be a slight decrease in electromagnetic power approaching the tap water in the cup centre. However, the penetration depths in 1% CMC solutions were much smaller than that for tap water, indicating power decay from the cup wall to the centre.

3.2. Heating uniformity in a horizontal plane

The horizontal heating uniformity at 4.5 cm height for the asymmetric design of conductor's and feed strip's positions as illustrated in Fig. 3a is shown in Fig. 4. A similar temperature distribution was observed for each test using different heating rates ranging from 3 to 9 °C min^{-1}. The hottest spot was always located at the central column C4, which was between the conductor and the feed strip (Fig. 4). The temperature difference along each column was less than 2 °C but the temperature difference along the rows was as much as 10 °C. There was a zone near the centre of the cavity in which the temperature difference was less than 4 °C. The dimension of the zone was about 35 cm × 70 cm. This uniform temperature zone was probably enough to develop a small-scale treatment protocol for dry products, such as walnuts or almonds, which have a wide temperature tolerance in quality. The mean temperature along the 4 rows, each including 6 cups, was very close (the standard deviation was around 1 °C) for all tests. The large temperature variations along each row (R1–R4) suggested that moving the samples on a convey belt along the row direction could improve the heating uniformity.

Heating uniformity for different areas (24, 16 and 4 cups) is summarized in Table 2. All six tests suggested that the smaller the area used, the more uniform the temperature obtained. The temperature distribution was repeatable over the replicates. The area could be selected for batch-type RF

Table 1 – Values (Ave ± Std) of dielectric constant (ε') and loss factor (ε'') and estimated penetration depths (d_p) for tap water and 1% CMC solutions at 27.12 MHz

Sample	Temp. (°C)	ε'	ε''	d_p (cm)
Tap water	20	77.5 ± 1.5	20.2 ± 0.1	77.9
	30	73.5 ± 0.9	23.4 ± 0.4	65.6
	40	68.6 ± 1.0	27.2 ± 0.5	55.0
	50	64.6 ± 0.9	31.1 ± 0.5	46.9
	60	61.4 ± 0.4	35.9 ± 0.4	40.2
1% CMC	20	85.4 ± 0.2	88.6 ± 0.5	20.4
	30	83.0 ± 0.4	103.1 ± 0.2	17.8
	40	80.8 ± 0.2	119.7 ± 0.2	15.7
	50	78.5 ± 0.1	136.4 ± 0.4	14.1
	60	76.1 ± 0.1	155.6 ± 0.1	12.7

treatments of different products based on the quality requirements for the temperature variations.

3.3. *Heating uniformity in the vertical plane*

Fig. 5 shows the measured temperatures of tap water in bottom, middle and top layers in cup 9 after RF heating. The water temperature in the three layers increased from about 20 to 50 °C in 30 s but was slightly separated after the initial ramp, which was probably due to heat convection in the cups. The water temperature in an individual cup was higher at the surface and lower at the bottom, which was similar to the results found by Zhong et al. (2003). The temperature differences between the three levels reduced only slightly during the natural cooling period because of limited heat loss from the cup. The maximum difference between the top and the bottom layer ranged from 2 to 4 °C in the water cups. The temperature distribution at the middle level of the cups in central columns C3 and C4 matched those obtained by the horizontal measurement system.

Fig. 6 shows the vertical temperature distribution of tap water in column C3 after RF heating for 3.3 min. The temperature layers were clearly separated from top (T) to bottom (B). The pattern showed that the temperatures at the far side were higher than those at the near side in column C3. The temperature distributions at the middle level matched those at the horizontal plane (Fig. 4). The maximum temperature difference at the three levels was 3 °C.

Fig. 7 shows the measured temperatures in 1% CMC solutions in the bottom, middle and top layers in cup 9 after removing from the RF system. The reverse temperature distribution and a much larger temperature difference (13 °C) among the three layers were observed as compared with those using tap water.

This difference was caused by a lack of natural convection in viscous 1% CMC solution. Therefore, the vertical temperature variation in the CMC solution truly reflected the intensity of electromagnetic field in the tested loads. Temperatures in the bottom layer were higher than those in the middle and top layers. This was probably caused by the limited penetration depth in 1% CMC solutions as indicated in Table 1. Since the RF power passed from the cup wall and bottom to the centre, the large power decay in 1% CMC solutions resulted in hotter layers around the cup wall and colder layers in the

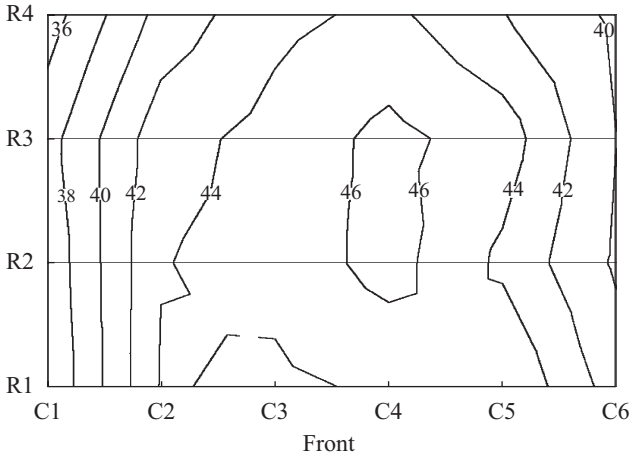

Fig. 4 – Horizontal temperature (°C) distribution at 24 cups when the gap was 175 mm after RF heating for 3.3 min with the original positions of conductors and feed strips.

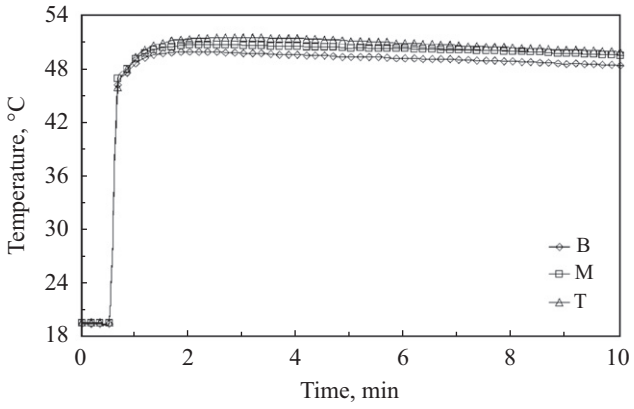

Fig. 5 – Measured temperatures of tap water in the bottom (B), middle (M) and top (T) layers in cup 9 after RF heating stopped.

Table 2 – Average (Ave.), standard deviation (Std.) and maximum difference (Max. dif.) values of the final water temperatures (°C) at the cup centre over different horizontal areas in the RF system

Tests	24 cups over 103 cm × 75 cm			16 cups over 64.8 cm × 64.8 cm			4 cups over 26.5 cm × 26.5 cm		
	Ave.	Std.	Max. dif.	Ave.	Std.	Max. dif.	Ave.	Std.	Max. dif.
1	41.4	2.8	10.7	42.9	1.4	5.7	44.3	1.1	2.5
2	42.3	3.4	12.1	44.3	1.5	5.6	45.9	1.1	2.2
3	42.2	3.4	11.8	44.2	1.6	6.1	45.7	1.2	2.2
4	43.7	3.5	12.1	45.8	1.4	5.4	47.1	0.5	1.2
5	40.5	3.4	11.7	42.4	1.8	6.3	44.3	1.2	2.3
6	42.6	3.4	11.8	44.6	1.5	5.4	45.7	1.0	2.4
Ave.	42.1	3.3	11.7	44.0	1.5	5.8	45.5	1.0	2.1

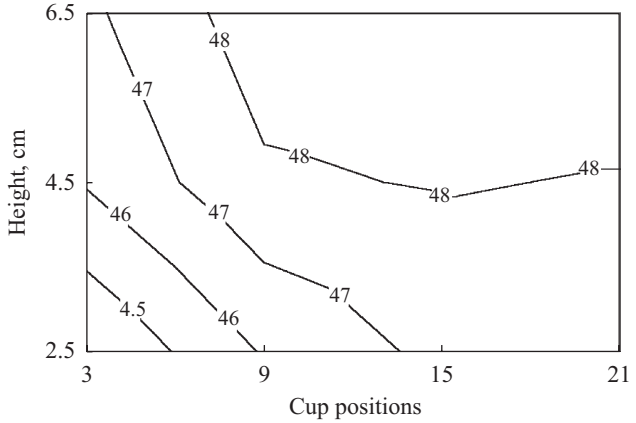

Fig. 6 – Vertical temperature (°C) distribution of tap water in column C3 after RF heating for 3.3 min.

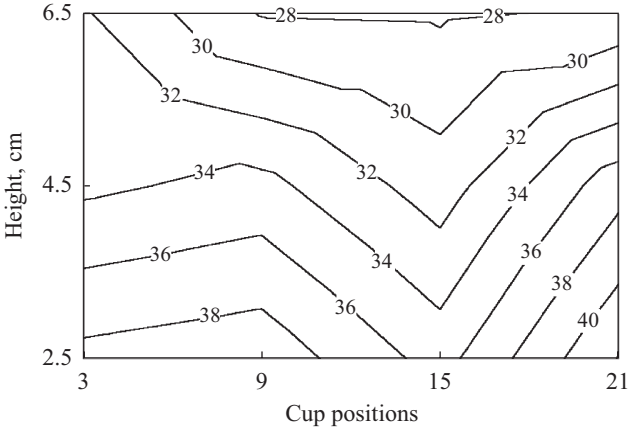

Fig. 8 – Vertical temperature (°C) distribution of 1% CMC solutions in column C3 after RF heating for 3.3 min.

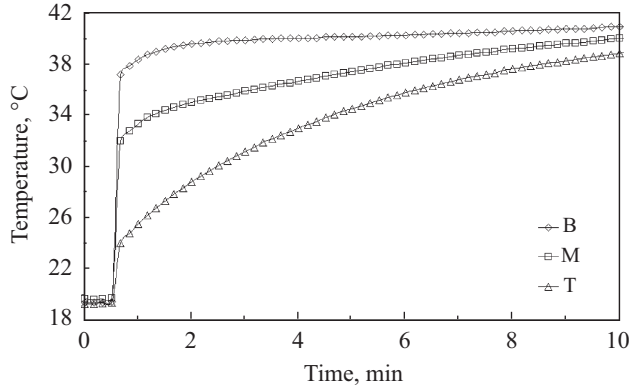

Fig. 7 – The measured temperatures of 1% CMC solutions in the bottom (B), middle (M) and top (T) layers in cup 9 after RF heating stopped.

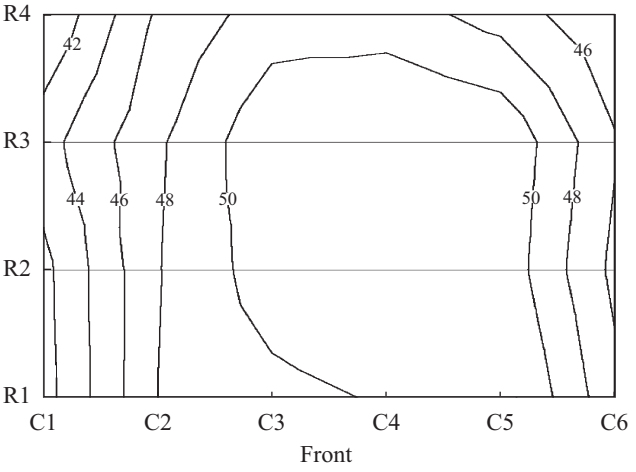

Fig. 9 – Horizontal temperature distribution at 24 cups when the gap was 175 mm after RF heating for 3.3 min with the new design of conductors and feed strips in the symmetric positions.

centre. Due to heat conduction, the temperatures in the middle and top layers increased gradually and approached the bottom temperature after the RF system had been turned off for 10 min. The bottom temperature did not decrease with time after RF heating, suggesting a possibly warmer spot closer to the bottom of the cup. Fig. 8 shows the vertical temperature distribution of 1% CMC solutions in column C3 after RF heating for 3.3 min. A similar vertical temperature pattern was observed in each cup. The maximum temperature difference between the top and bottom layers was 6–7 °C.

The large penetration depth and natural heat convection make the water load suitable for evaluating the overall horizontal heating uniformity in RF systems. But the 1% CMC solution should be used to determine the vertical heating uniformity because its viscous property eliminates natural convection experienced in water.

3.4. *Heating uniformity improvement using the symmetric design*

Fig. 9 shows the horizontal water temperature distribution with the symmetric design of the conductor's and feed strip's positions as illustrated in Fig. 3b for the middle heights of 24 cups when the gap was 175 mm after RF heating for 3.3 min. Although the maximum temperature difference was still as high as 10 °C, the temperature zones with less than 4 and 2 °C difference now extended over areas of 70 cm × 70 cm and 50 cm × 50 cm, respectively. The temperature distribution was further confirmed by thermal imaging of the foams (Fig. 10). Although the final temperatures (58–60 °C) in Fig. 10 were higher than those (50–52 °C) in Fig. 9 due to different thermal and dielectric properties, the heating patterns were similar for both the water loads and the polyurethane foams. The zones with less than 4 and 2 °C temperature difference were observed again near the centre but slightly toward the front and right sides of the electrodes. The heating uniformity was improved based on the field distribution beneath the applicator of the RF heater and was acceptable for pilot-scale treatment of agricultural products in the defined area.

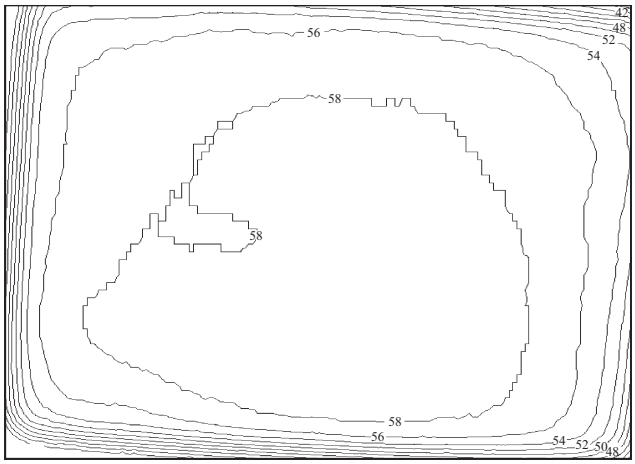

Fig. 10 – Horizontal temperature distribution over polyurethane foams using thermal imaging when the gap was 160 mm after RF heating for 3 min with the new design of conductors and feed strips in the symmetric positions.

4. Conclusions

A uniform heating load developed in this study was used to determine the horizontal and vertical temperature distributions in a pilot-scale RF system. The hottest spot was always located at the electrode centre which was between the conductor and the feed strips. The temperature difference between the front and back was less than 2 °C but the value between the right and left sides was as much as 10 °C. A zone of 35 cm × 70 cm can be defined in the centre where the temperature difference was less than 4 °C. Based on vertical temperature measurements, the temperature gradient across the 1% CMC solutions was larger than that observed in tap water due to RF power decay, suggesting that more uniform heating can be achieved in low loss factor materials than that in high loss factor materials. The symmetric design of inductance positions and feeding strips improved the heating uniformity by increasing the zones with 4 °C differences to 70 cm × 70 cm.

Acknowledgements

This research was supported by grants from USDA-CSREES (2004-51102-02204), USDA-NRI (2005-35503-16223), and Washington State University IMPACT Centre. We thank Tony Koral (Strayfield International Limited, Wokingham, UK) for his useful suggestions and technical support.

REFERENCES

Birla S L; Wang S; Tang J; Fellman J; Mattinson D; Lurie S (2005). Quality of oranges as influenced by potential radio frequency heat treatments against Mediterranean fruit flies. Postharvest Biology and Technology, **38,** 66–79

Birla S L; Wang S; Tang J; Hallman G (2004). Improving heating uniformity of fresh fruits in radio frequency treatments for pest control. Postharvest Biology Technology, **33,** 205–217

Frings H (1952). Factors determining the effects of radio-frequency electromagnetic fields and materials they infest. Journal of Economic Entomology, **45,** 396–408

Hallman G J; Sharp J L (1994). Radio frequency heat treatments. In: Quarantine Treatments for Pests of Food Plants (Sharp J L; Hallman G J, eds), pp 165–170. Westview Press, San Francisco, CA

Headlee T J; Burdette R C (1929). Some facts relative to the effect of high frequency radio waves on insect activity. Journal of New York Entomology Society, **37,** 59–64

Ikediala J N; Hansen J D; Tang J; Drake S R; Wang S (2002). Development of saline-water-immersion technique with RF energy as a postharvest treatment against codling moth in cherries. Postharvest Biology Technology, **24,** 25–37

Jia X (1993). Experimental and numerical study of microwave power distributions in a microwave heating applicator. Journal of Microwave Power Electromagnetic Energy, **28,** 25–31

Jones P L (1997). RF heating, an old technology with a future. In: Microwave: Theory and Applications in Materials Processing IV (Clarck D E; Sutton W H; Lewis D A, eds), pp 261–268. The American Ceramic Society, Westerville, Ohio

Ma L; Paul D L; Pothecary N; Railton C; Bows J; Barratt L; Mullin J; Davis S (1995). Experimental validation of a combined electromagnetic and thermal FDTD model of a microwave heating process. IEEE Transactions of Microwave Theory Techniques, **43,** 2565–2572

Mataxas A C; Clee M (1993). Coupling and matching of radio frequency industrial applicators. Power Engineering Journal, **7,** 85–93

Mitcham E J; Veltman R H; Feng X; de Castro E; Johnson J A; Simpson T L; Biasi W V; Wang S; Tang J (2004). Application of radio frequency treatments to control insects in in-shell walnuts. Postharvest Biology and Technology, **33,** 93–100

Nelson S O (1972). Insect-control possibilities of electromagnetic energy. Cereal Science Today, **17,** 377–387

Nelson S O (1996). Review and assessment of radio-frequency and microwave energy for stored-grain insect control. Transactions of the ASAE, **39,** 1475–1484

Nelson S O; Payne J A (1982). RF dielectric heating for pecan weevil control. Transactions of the ASAE, **31,** 456–458

Tang J; Ikediala J N; Wang S; Hansen J D; Cavalieri R P (2000). High-temperature-short-time thermal quarantine methods. Postharvest Biology Technology, **21,** 129–145

Wang S; Ikediala J N; Tang J; Hansen J D; Mitcham E; Mao R; Swanson B (2001). Radio frequency treatments to control codling moth in in-shell walnuts. Postharvest Biology Technology, **22,** 29–38

Wang S; Monzon M; Johnson J A; Mitcham E J; Tang J (2007a). Industrial-scale radio frequency treatments for insect control in walnuts: I. Heating uniformity and energy efficiency. Postharvest Biology and Technology, **45,** 240–246

Wang S; Monzon M; Johnson J A; Mitcham E J; Tang J (2007b). Industrial-scale radio frequency treatments for insect control in walnuts: II. Insect mortality and product quality. Postharvest Biology and Technology, **45,** 247–253

Wang S; Tang J; Johnson J A; Mitcham E; Hansen J D; Cavalieri R P; Bower J; Biasi B (2002). Process protocols based on radio frequency energy to control field and storage pests in in-shell walnuts. Postharvest Biology Technology, **26,** 265–273

Wang S; Tang J; Johnson J A; Mitcham E; Hansen J D; Hallman G; Drake S R; Wang Y (2003a). Dielectric properties of fruits and insect pests as related to radio frequency and microwave treatments. Biosystems Engineering, **85,** 201–212

Wang S; Yue J; Tang J; Chen B (2005). Mathematical modeling of heating uniformity of in-shell walnuts in radio frequency units with intermittent stirrings. Postharvest Biology and Technology, **35,** 94–104

Wang Y; Wig T; Tang J; Hallberg L M (2003b). Radio frequency sterilization of packaged foods. Journal of Food Science, **68,** 539–544

Zhong Q; Sandeep K P; Swartzel K R (2003). Continuous flow radio frequency heating of water and carboxymethylcellulose solutions. Journal of Food Science, **68,** 217–223

Zhou L; Puri V M; Anantheswaran R C; Yeh G (1995). Finite element modeling of heat and mass transfer in food materials during microwave heating- model development and validation. Journal of Food Engineering, **25,** 509–529